Original Paper

Evaluation of bubble removing performance in a TV glass furnace

Part 2. Verification using real furnace data[1)]

Shinji Kawachi

Technology Department, Nippon Electric Glass Co. Ltd., Otsu, Shiga (Japan)

Yoshinori Kawase

Department of Applied Chemistry, Toyo University, Kawagoe, Saitama (Japan)

In part 2, a furnace for melting TV panel glass is studied to examine the effectiveness of the simulator developed by the authors. Because panel glass is used as a part of a cathodic ray tube where the TV image is projected and its defect is easily recognizable, bubble-free glass quality is definitely required. If the bubble quality becomes worse, a heap of rejected products is piled up, which leads to tremendous economical loss. In order to avoid such trouble designing and operating a TV glass furnace and inspecting glass quality are conducted with great care, and therefore, lots of field data have been accumulated so far. Accordingly, it is meaningful to utilize a TV glass furnace to verify the effectiveness of such simulating technology. The values and phenomena predicted by the simulator and the data having been observed in real furnaces were found to be in reasonable agreement. Therefore, it may be concluded that the proposed simulator is useful as a method of scale-up and trouble-shooting for glass furnaces.

Beurteilung der Effizienz der Blasenentfernung bei einem Schmelzofen für Fernsehröhrenglas. Teil 2. Überprüfung an Hand realer Ofendaten

Im vorliegenden Teil 2 der Arbeit wird ein Ofen zum Schmelzen von Bildschirmglas für Fernsehgeräte untersucht, um die Wirksamkeit des von den Autoren entwickelten Simulators zu überprüfen. Da der Bildschirm ein Teil der Kathodenstrahlröhre ist, auf dem das Fernsehbild erzeugt wird, und Fehler leicht erkannt werden können, ist ein absolut blasenfreies Glas erforderlich. Eine Veränderung der Eigenschaften der Blasen kann zu einer großen Menge von Ausschußware und damit zu hohen wirtschaftlichen Verlusten führen. Um derartige Probleme zu vermeiden, werden der Aufbau und die Betriebsweise von Schmelzöfen für Fernsehröhrenglas sowie die Qualitätskontrolle des Glases sehr sorgfältig überwacht, wodurch sich schon zahlreiche Einzeldaten angesammelt haben. Es ist also sinnvoll, die Wirksamkeit einer solchen Simulationstechnik an einer Wanne für Fernsehglas zu überprüfen. Als Ergebnis der Simulation konnte festgestellt werden, daß die vom Simulator vorhergesagten Werte und Phänomene mit den an vorhandenen Öfen erhaltenen Daten in befriedigender Weise übereinstimmen. Man kann daher davon ausgehen, daß der Einsatz des vorgeschlagenen Simulators ein anwendbares Verfahren für die Störungssuche und -beseitigung bei Glasschmelzöfen ist.

1. Verification of the bubble removing theory in a TV glass furnace

1.1 Objective of the model

A series of tests were conducted to verify the principles proposed in part 1 [1] in a TV panel glass furnace as a case study. Because panel glass is used where the TV image is projected, even one bubble larger than the specification becomes a cause for reject. Consequently, one of the most difficult tasks for manufacturers of glass for cathodic ray tubes is the production of bubble-free glass.

The authors used a side-fired tank (see figure 1 in [1]) consisting of a melter and a refiner with a throat between the chambers. The melter is heated by burning fuel oil in the hot air preheated by a regenerator. The refining chamber is cooled or only slightly heated with petroleum gas because the thermal energy brought into the refiner with the molten glass from the melter is generally excessive. Two feeders are connected to the refiner. Because the feeders are thought to have little effect on the bubble removing performance, the border of the refiner to these feeders is regarded as the end of this system.

The pull rate is 180 t/d and the surface of the bath is assumed to be uniformly covered with the batch up to 40 % length from the charging end.

Figure 1 shows an outside view of the model. In most cases the calculation results will be presented in the center section hereafter, shown with a lozenge mesh to clarify the characteristics of this model. Since the shadowed part in the refining chamber means an obstacle cell in the present program code, it indicates that the furnace width narrows in the real refining chamber.

1.2 Thermal fluid analysis

To begin with, the glass flow and the temperature distributions in the tank were computed as shown in the sub-

Received June 18, revised manuscript December 3, 1997.

[1)] Part 1. Mathematical formulation. Glastech. Ber. Glass Sci. Technol. **71** (1998) no. 4, p. 83–91 [1].

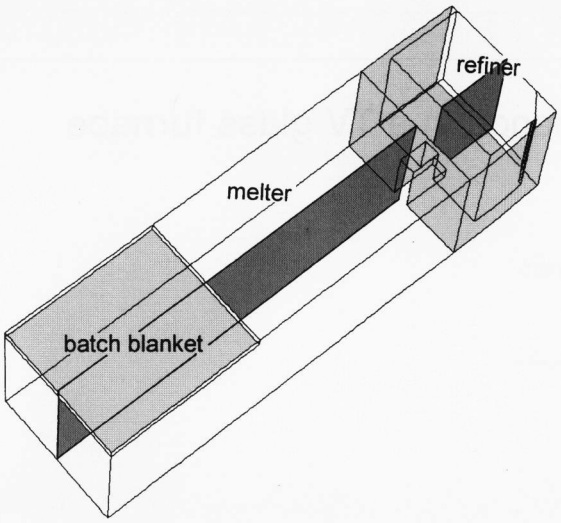

Figure 1. Bird's eye view of a glass furnace model.

models and the calculation procedure of figure 2 in [1]. The results of the thermal fluid analysis are shown in figures 2a to f.

Figure 2a depicts the temperature distribution at the surface according to measurements in a real TV furnace. This distribution was adopted as the boundary condition of heat. The highest temperature is kept at 1550 °C in the furnace center and the temperature is lowered gradually in the direction of the throat, reaching 1500 °C at the bridge wall. Incidentally, the temperature starts at 1420 °C in the vicinity of the batch entrance.

Figure 2b indicates the calculated velocity pattern at the uppermost plane. Figures 2c through f are views of the center section of the furnace. To make the figures easy to understand, the depth dimension is enlarged five times.

In the velocity distribution at the surface in figure 2b, a hot spring is observed and the flow is separated into two directions, one going toward the charging end and the other toward the bridge wall. In the refining chamber, the flow which comes through the throat tunnel extends radially on the surface.

Figure 2c indicates the temperature distribution and figure 2d the velocity distribution in the center section. As seen from figure 2d, in the throat tunnel, there exist two flows of forward moving current caused by the glass pull and the back current caused by the temperature difference between the melter and the refiner. Since the back current with a low temperature re-enters the melter, the bottom temperature in the melter decreases to about 1400 °C.

In figure 2e the movement of marker particles set throughout the whole volume of the glass melt is shown. The marker particles moved for a short period of time with the flow to visualize the flow pattern more clearly. A part of the flow (rather unclear in figure 2d) can be viewed by such a technique.

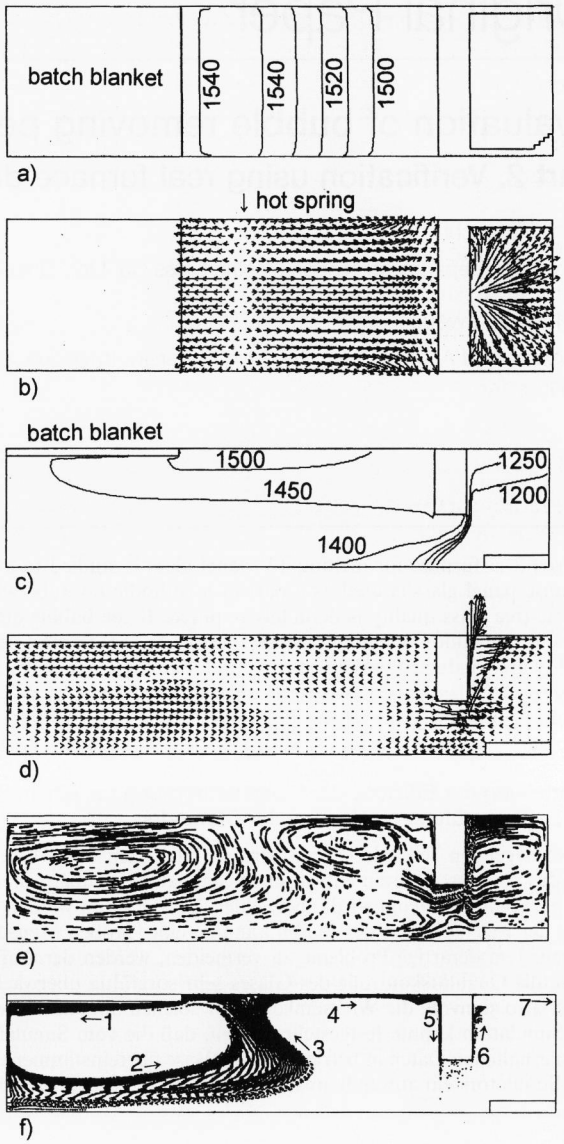

Figures 2a to f. Boundary condition and results of thermal fluid analysis, a) temperature distribution at the surface of the glass melt, boundary condition from measured data; b) velocity pattern at the uppermost plane; c) temperature at the central section in °C; d) velocity at the central section; e) flow pattern at the central section observed by particle tracing method; f) particle trajectory started from beneath batch blanket.

Figure 2f represents particles evenly distributed beneath the batch blanket and moved until the fastest particle reaches the outlet, i.e. the feeder entrance. The particles placed beneath the batch tend to return toward the side blocks of the batch charging end (1 in figure 2f) and descend along them. They creep along the bottom and approach the hot spring zone (2 in figure 2f). The main flow rises to the surface (3 in figure 2f), proceeds to the neighborhood of the surface (4 in figure 2f) and is drawn into the throat (5 in figure 2f). The particles passing through the throat ascend rapidly upon entering the refiner (6 in figure 2f), flow near the surface and proceed to the outlet (7 in figure 2f). On the other hand, the

flow which rises in the hot spring goes toward the batch charging end simultaneously with the flow moving toward the throat side. It is said that the flow toward the charging end plays an important role in preventing a short cut flow to the bridge wall by retaining batch at the batch charging side [2].

1.3 Calculation of gas partial pressure

In the next step, the concentration of gas dissolved in each place in the glass melt is to be determined. For this purpose the three values described in section 2.1 of part 1 [1] are needed.

1.3.1 Gas generated by refining agents

The refining agent weighing 0.3 % of glass is employed in the form of antimony trioxide. To convert the antimony trioxide to antimony pentoxide at a comparatively low temperature, a sufficient amount of nitrate is added to the batch in advance. Cullet, with a batch ratio of 35 %, does not influence the oxygen generation from the refining agent included in it. At the pull rate of 180 t/d, $4.062 \cdot 10^{-3}$ kg/s of the refining agent is charged.

In order to construct a batch reaction model that describes the gas evolution from refining agents as a function of time and temperature, equations (5 through 7) (see part 1 [1]) are utilized. For the purpose of obtaining the refining gas amount at a certain temperature and elapsed time three parameters must be fixed by gas profile measurement. In the measuring method, a certain amount of batch is heated at a constant heating rate and the generated gases are quantitatively measured [3].

Figure 3 shows the measurement results of the batch and the cullet of TV glass used for this study. The difference of curves 1 and 3 was the truly evolving gas by the refining agent. The three parameters obtained from this measurement were computed as follows [4]:

- frequency factor: $A = 2.347 \cdot 10^{11}\ s^{-1}$,
- activation energy: $E = 4.247545 \cdot 10^{5}$ J/mol,
- reaction degree: $n = 3.868$.

Curve 2 is the result of the gas profile measurement of cullet-containing refining agent. The cullet is glass melted in a real TV furnace with substantially the same thermal history as an average glass melt, ranging from the highest temperature, i.e. the melting temperature, to the lowest temperature, i.e. the forming temperature. The measurement result does not show any oxygen evolution as observed in curve 1.

It is believed that, when the glass is cooled, antimony trioxide at high temperature is converted to antimony pentoxide in the reaction with oxygen dissolved in the molten glass, which is useful as a bubble removing measure called the 'setting' effect. From curve 2, however, no proof is observed that the antimony oxide in TV glass cullet is in a pentavalent state. It is because, if the antimony oxide in the cullet is in the state of pentavalency, oxygen evolution should have been observed like in curve 1 when the cullet is heated. There is a slight deviation at 1450 °C from curve 2, which might mean that some antimony oxide is in a pentavalent state. But, even if this is true, oxygen generation is very small in comparison with that of decomposition of batch containing a refining agent. Therefore, it is sufficient to consider only the decomposition reaction caused by heating.

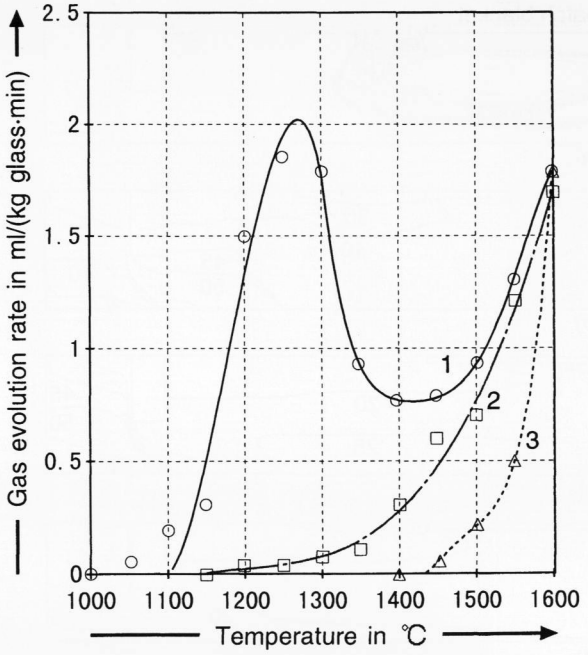

Figure 3. Gas profile measurement on TV panel glass batch and cullet. Curve 1: batch including refining agent, curve 2: cullet including refining agent, curve 3: batch without refining agent.

The glass converted from the batch moves in the furnace as shown in figure 2f. Using the above-mentioned conditions, the oxygen evolution in the furnace was computed. This result is illustrated at the center section in figure 4a. Obviously, the glass including a refining agent violently generates oxygen beneath the batch blanket. As the glass advances in the direction of the furnace bottom, the gas generation rate temporarily declines. When the glass proceeds to the center of the furnace, it is raised from the bottom to the surface. As the glass goes by, the temperature rises and the oxygen generation becomes vigorous again. The surface glass having passed the hot spring and going to the bridge wall still continues to generate oxygen. The amount of oxygen evolved at each location in the furnace is provided according to this procedure.

1.3.2 Conditions at batch/glass melt boundary

As one of the boundary conditions shown in the chart of figure 3 in [1], it is necessary to prepare the gas concentration at the batch/glass melt boundary. The values of the gas concentration according to the following method are used. The batch pile formed in the furnace is observed to dissolve and disappear in about 30 min in

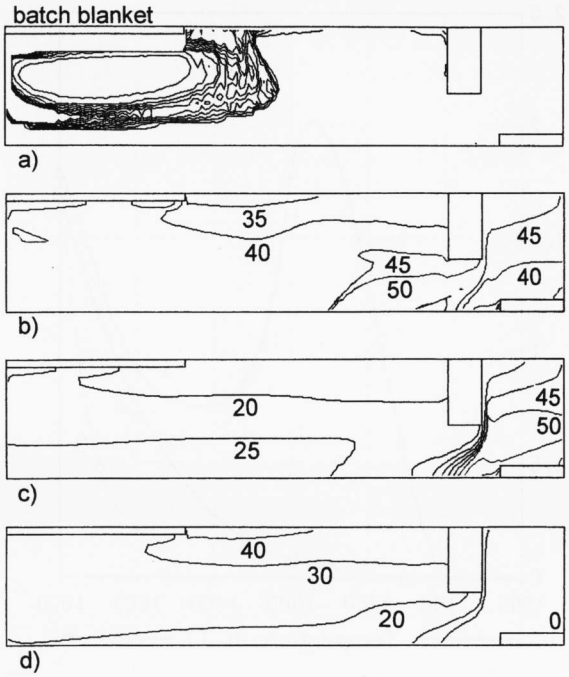

Figures 4a to d. Distribution of oxygen evolution by refining agents and concentration of gases; a) evolution of oxygen due to decomposition of refining agents; b) concentration of CO_2 in the melts (in wt%), c) concentration of N_2 in the melts (in wt%), d) concentration of O_2 in the melts (in wt%).

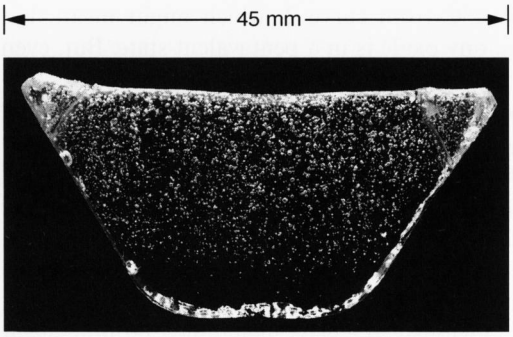

Figure 5. Outside view of initial glass.

a real TV furnace. Accordingly, in terms of CO_2 and O_2, the batch is melted in a crucible with the same thermal history as the batch pile, and the amount of dissolved gas in the initial glass is measured. As for N_2, the solubility at the batch melting temperature is adopted because of the limited sensitivity of the measuring device. The amounts of gases (in kg/m^3) in the initial glass applied are: $4.0 \cdot 10^{-3}$ CO_2, $3.0 \cdot 10^{-4}$ N_2, $6.7 \cdot 10^{-2}$ O_2.

1.3.3 Conditions at molten glass/combustion space boundary

The gas concentration where the combustion gas contacts the glass melt is needed as the boundary condition of gas as illustrated in figure 3 (see part 1 [1]). The gas composition in the combustion space of a side-port furnace is different at each location on the glass surface. A small difference in the gas composition at different glass surface locations has been known to have a slight influence on the distribution of gas concentration in the molten glass. The average composition(in vol.%) of 18 CO_2, 80 N_2, 2 O_2 is adopted from the measurement in a real operating furnace.

1.3.4 Distribution of gas partial pressure

Figures 4a to d show the solution of equation (4 in [1]) where the source term condition in section 1.3.1 and the boundary conditions in sections 1.3.2 and 1.3.3 are used. Figures 4b to d indicate the gas concentration of CO_2, N_2 and O_2 in the center section of the furnace.

Although oxygen evolution due to the decomposition of antimony pentoxide is violent within the convection current from the batch layer, it is understood that both effects of the diffusion and the flow make the evolved oxygen diffuse more evenly. The surface of the glass in the melting chamber is comparatively rich in oxygen, but the oxygen content in refiner glass becomes very poor.

Mulfinger [5] discussed the glass collected from each part of a borosilicate glass furnace, where antimony or arsenic oxide was used with nitrate, like for a panel glass, and reported the analytical results of the bubble gas. The paper stated that bubbles gathered from the bath surface contained a lot of oxygen, and bubbles from the glass in the refiner and from the product were poor in oxygen. Because the partial pressure of gas in the glass melt is thought to be proportional to the gas composition of the bubble, this analytical result is in reasonable agreement with the results of the present simulation. Furthermore, the authors' analyses of gas bubbles in samples from the surface of the glass melt as well as from products showed the same tendencies as given in Mulfinger's paper.

1.4 Calculation of bubble removing process

1.4.1 Determination of characteristics of initial bubbles

As is noted in section 1.3.2, the batch pile dissolves and disappears in about 30 min in a real TV furnace, and becomes the initial glass melt which contains a huge number of bubbles. In accordance with the above information, the following glass melt was made to represent this initial glass.

The batch was put in a platinum crucible to obtain about 100 g glass, and was heated for 30 min at 1400 °C. The glass was cooled quickly to the vicinity of the annealing point to freeze-in the state at high temperature, and was left for natural cooling afterwards. It was sliced to 3 mm in thickness and was polished on the surface. Figure 5 is the photograph of the glass sample. The diameter distribution of the initial bubbles was measured with an image processor and the result is shown in figure 6. In addition, the gases in the bubble were analyzed

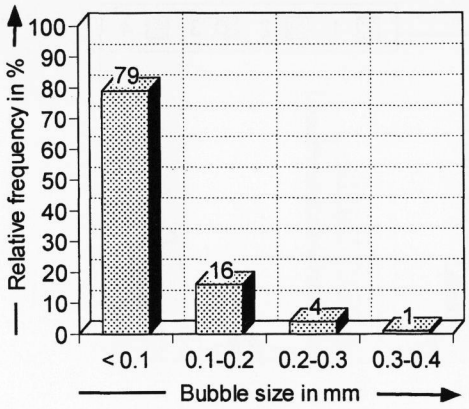

Figure 6. Diameter distribution of initial bubbles.

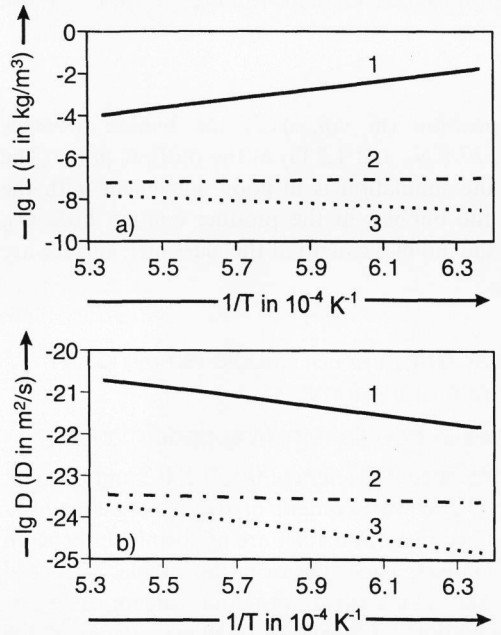

Figures 7a and b. Solubility and diffusivity of TV panel glass; a) solubility, curve 1: O_2, curve 2: CO_2, curve 3: N_2; b) diffusivity, curve 1: O_2, curve 2: CO_2, curve 3: N_2.

by gas chromatography, which resulted in the following average composition (in vol.%): 15.7 CO_2, 0.3 N_2, 84.0 O_2.

1.4.2 High-temperature properties needed for calculating the bubble removing process

To predict the bubble behavior, such as growth and shrinkage in the glass melt, gas solubility, gas diffusivity, and surface tension are needed as a function of temperature. The data shown in figures 7a and b was used for the panel glass of this paper with regard to solubility and diffusivity.

The surface tension was constant at 0.2805 N/m in this simulation. There was almost no change within the temperature range of 1400 to 1500 °C, according to the authors' measurements.

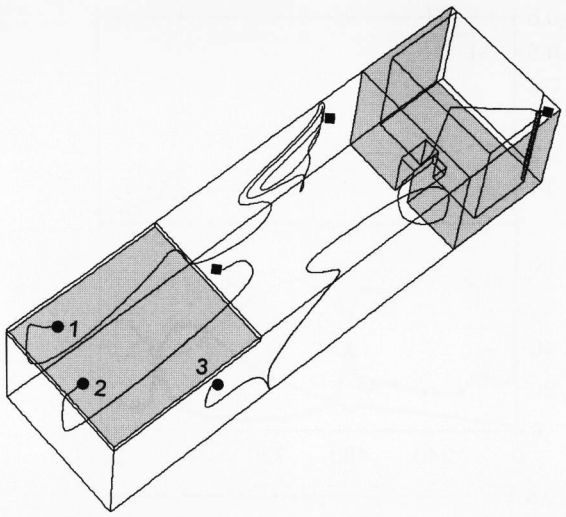

Figure 8. Example of trajectory of bubble movement, ●: starting point, ■: arrival point. 1: bubble removal because of absorption, 2: bubble disengagement because of flotation, 3: bubble flow out from refiner.

1.4.3 Trajectory of initial bubbles

The bubbles originating from beneath the batch blanket will develop into one of the following situations after a period of time.

a) The bubbles are removed due to the absorption of the bubble gases into the melt.

b) The bubbles are also eliminated by flotation.

c) The bubbles flow into the feeder and might be included in glass products.

d) The bubbles remain in the furnace.

Figure 8 represents the trajectory of three initial bubbles, whose gas composition (in vol. %) and size are 15.7 CO_2, 0.3 N_2, 84.0 O_2, and 0.4 mm in diameter, respectively. In the figure, the mark ● means the starting point of three bubbles and the mark ■ indicates their arrival point. Figures 9a to c indicate the change in the diameter and the gas composition of these bubbles. Figure 9a is an example of the disappearance of a bubble due to absorption. The initial bubble with a diameter of 0.4 mm becomes smaller, down to about 0.2 mm, absorption of O_2 taking place rapidly. In addition, as the bubble moves, it continues to shrink and at last becomes less than 0.001 mm in diameter which is regarded as the temporary criteria of disappearance by absorption. Finally, the bubble becomes rich in CO_2 and N_2, and poor in O_2.

Figure 9b shows an example of the disengagement of a bubble due to flotation. Once the bubble moves in the direction of the bottom, the bubble diameter decreases, but it increases again as it approaches the surface. As the bubble diameter grows, the buoyancy of the bubble becomes greater, which accelerates the bubble removing function. The bubble reaches the surface with abundant

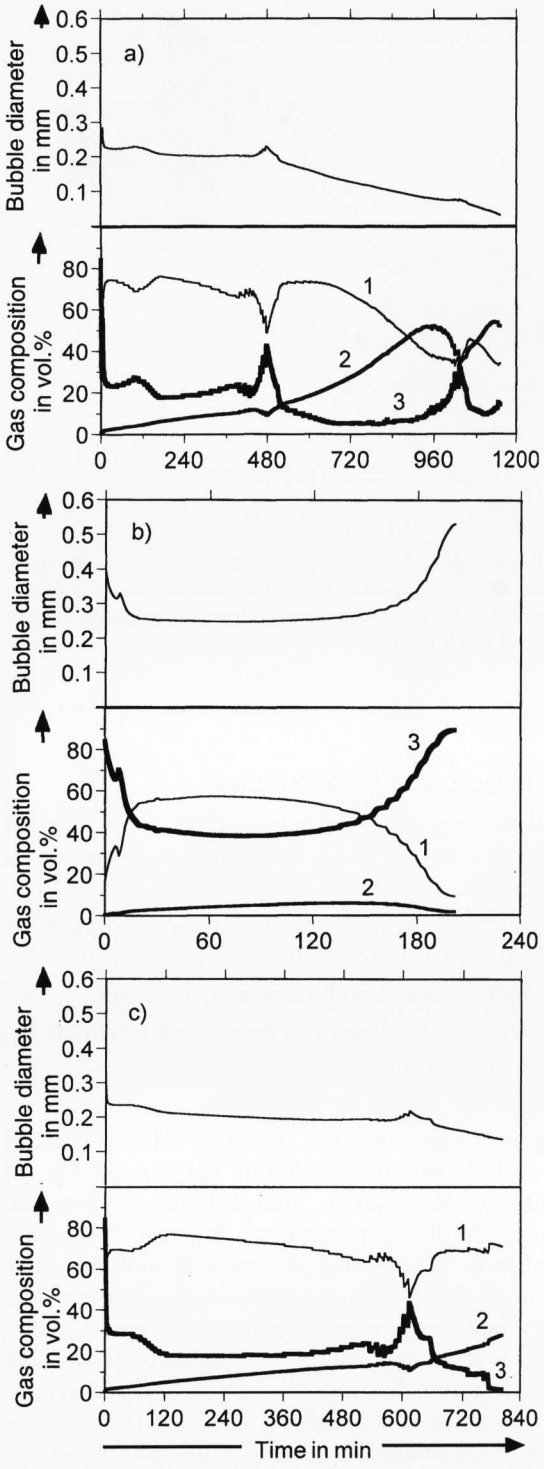

Figures 9a to c. Change of bubble diameter and gas composition, curve 1: CO_2, curve 2: N_2, curve 3: O_2; a) bubble removal because of absorption, b) bubble disengagement because of flotation, c) bubble flow out from refiner.

O_2, and little CO_2 and N_2. This well explains the authors' experience that glass scooped up from the bath surface contains much O_2.

Figure 9c is an example in which a bubble flows out of the refiner without disappearing in the furnace. The

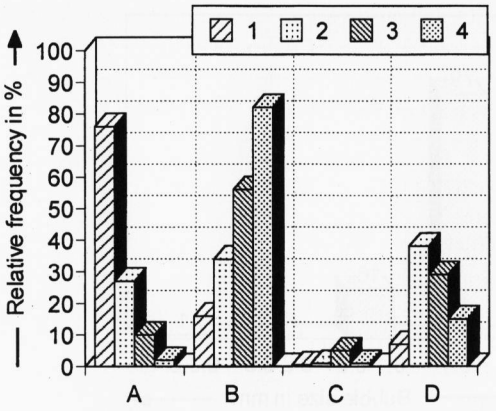

Figure 10. Behavior of bubbles after 24 h as a function of the initial bubble size. A: removed due to absorption, B: removed due to flotation, C: removed due to flow out, D: remaining. Initial bubble diameter (in mm): 1: 0.1, 2: 0.2, 3: 0.3, 4: 0.4.

gas composition (in vol.%) of the bubble becomes 70.9 CO_2, 27.8 N_2 and 1.3 O_2 at the outflow point. The result of the simulation is in good agreement with the fact that the bubbles in the product contain little O_2, although the bubbles caught at the glass melt surface are rich in O_2.

1.5 Overall evaluation of bubble removing performance of the furnace

1.5.1 Index of bubble removing performance

2000 bubbles with diameters of 0.1, 0.2, 0.3 and 0.4 mm, respectively, and with content of the same gas composition as stated in section 1.4.1 are uniformly set beneath the batch blanket. The behavior of the bubbles is tracked for 24 h, and is classified into four categories as explained in section 1.4.3. Figure 10 shows the fate of the bubbles based on such classifications.

As it is clear from the figure, the smaller the size, the more easily the gas in the bubble is absorbed and the bubbles disappear. That is, 76.3% of the initial bubbles of 0.1 mm in diameter are removed by absorption, but only 1.6% of initial bubbles of 0.4 mm in diameter disappear by absorption. Bubbles with larger diameter disappear easily by flotation rather than absorption. That is, 82.3% of initial bubbles of 0.4 mm in diameter disappear due to flotation, although only 16.4% of initial bubbles of 0.1 mm in diameter are removed by the same cause.

It is hypothesized as a criterion to evaluate furnace performance in terms of bubble removal that the greater the numbers of bubbles which disappear by flotation and absorption, the better the performance of the furnace in the bubble removing process. Bubbles remaining in the furnace after 24 h have a possibility of disappearing due to flotation or absorption. However, there it is also possible that they will accumulate in the furnace and flow out in the products. Considering the minimum residence

time is 10 h for the furnace in question, the bubbles will stay up to 2.4 times longer. Accordingly, there will be the possibility to evaluate the bubble removing performance of the furnace by the sum of bubbles buoyed up and absorbed.

The existence ratio of the initial bubbles classified by the diameter is shown in figure 6. The numbers of bubbles which are removed by flotation or absorption depend upon the initial bubble size as is shown in figure 10. Then, the 'weighted disappearance index', i.e. the product of the existence ratio of the initial bubbles and the number of the bubbles that disappeared, is supposed to represent the bubble removing performance of the furnace. That means that 86.5% of the initial bubbles are removed within 24 h. This index should be used to evaluate the superiority or inferiority of various furnace situations, but its absolute value should not be emphasized.

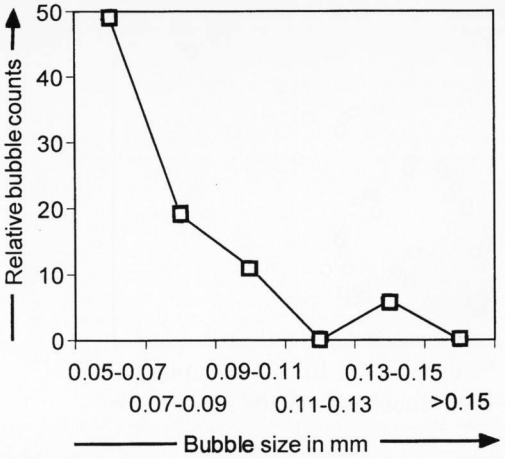

Figure 11. Predicted relative diameter distribution of bubbles which flow out from refiner and are larger than 0.05 mm in diameter.

1.5.2 Diameter distribution of outflow bubbles

The reject bubble for panel glass is assumed to be larger than 0.05 mm in diameter. The simulation indicates that the portion of the bubbles in this category is 0.325% of all bubbles generated at the initial stage of melting. The relative frequency of diameters of the outflow bubbles is predicted as shown in figure 11. It demonstrates that the maximum diameter of bubbles which passed through the furnace is 0.15 mm and the chance of a bubble to appear in products becomes higher as the size of the bubble gets smaller.

Figure 12 is the bubble size distribution confirmed in actual products. In each of three cases, the number of bubbles of 0.1 to 0.2 mm in diameter changed greatly according to the bubble quality of products. The reason that the bubbles of 0.1 mm or less did not change so much might be attributed to the difficulty of inspection with the naked eye. Comparing the value predicted in figure 11 with the measured one in figure 12, it can be concluded that this simulation correctly shows the bubble size which should be paid attention to.

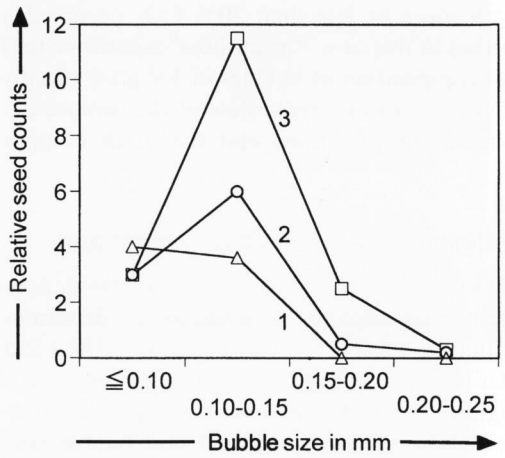

Figure 12. Actual bubble size distribution. Curve 1: case of excellent bubble quality, curve 2: case of intermediate bubble quality, curve 3: case of normal bubble quality.

1.5.3 Gas composition distribution of outflow bubbles

By measuring the CO_2 content in the outflow bubbles and making a histogram concerning the frequency of appearance, the distribution shown in figure 13 is obtained. Because most O_2 in the bubbles which reach the refiner outlet is absorbed, bubbles found in final products contain only CO_2 and N_2. Consequently, the characteristics of bubbles can be represented by the CO_2 content. Curve 1 in the figure plots the CO_2 distribution based on this simulation. Curves 2 and 3 show the actual results in panel glass, where the data of production and furnace were different. In curve 2, the bubbles with a slight CO_2

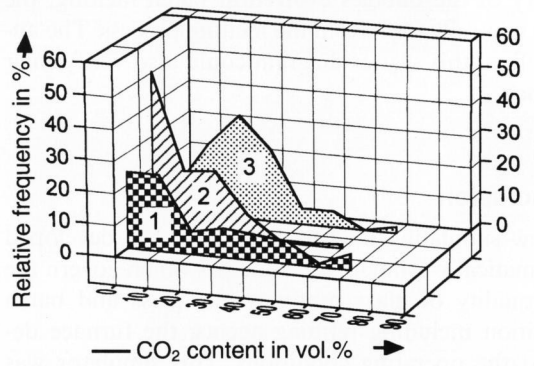

Figure 13. CO_2 gas distribution of bubbles which passed through the furnace. Curve 1: predicted results by the present simulation, curves 2 and 3: actual bubble data for different furnace design and production data.

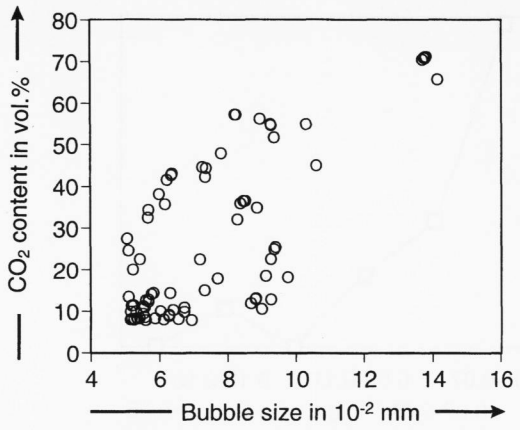

Figure 14. Predicted relation between CO_2 content and bubble size.

content were in the major portion. The bubble ratio decreased with an increase in CO_2. In contrast, in curve 3, the bubbles with about 20% CO_2 were in the majority. Bubbles with more or less than 20% CO_2 occupied a smaller portion in this case. The authors' experience tells that the gas composition of bubbles in TV glass usually varies within such a range regardless of the furnace design, the operating conditions and the batch composition.

1.5.4 Relationship between CO_2 content and bubble size

Bubble origin is occasionally searched for by determining the relation between the bubble gas composition and the diameter [6]. When the relationship is expressed in a scatter diagram, for instance, and if a negative correlation is found between CO_2 content and bubble size, the bubble is presumed to have originated from near the forming section. In the case of a positive correlation, the bubble occurred supposedly during the melting process.

The scatter diagram of figure 14 can roughly be read to mean that there exists a positive correlation. Because this simulation was originally developed to trace the trajectory of the bubbles evolved at batch melting, the bubbles naturally stem from the melting process. The authors believe this scatter diagram could also verify their experience.

2. Conclusion

a) A new simulating methodology has been developed to systematically estimate three factors which govern the bubble quality of glass products: the glass and batch composition including refining agents, the furnace design and the operating conditions. This simulator was applied to a furnace melting TV panel glass, and it was found to be in reasonably good agreement with the measured results from actual furnaces and the authors' experience as well.

b) As is understood from the flow chart of the calculation, the above three factors do not affect the bubble quality independently. In other words, there is an interdependent relationship among them. The bubble quality could be improved by revising the batch composition and operating conditions, even if there are some weak points in the furnace design.

c) It is preferable that a tank furnace should be operated at a lower temperature from the viewpoint of environmental protection, energy saving and longer furnace life. However, it is glass engineers' consensus that there is a risk of worsening the bubble quality. Using a bubble-removing simulator, the conditions for keeping high bubble quality can be investigated beforehand, even if the operating temperature is reduced.

d) The scale-up method, i.e. the performance of a large-scale device can be predicted with a small device, has not explicitly been applied up to now in developing glass melting furnaces. This might be attributed to the difficulty to find the similarity conditions, particularly in bubble quality, one of the most important qualities in glass production. It may be possible to scale-up the result of observations and measurement in a small tank for the design and operation of a large-scale furnace by deciding simulation parameters described in this paper. The authors believe that this method provides new possibilities as a research and development technique for the glass melting furnace.

e) In the example verifying this simulation, bubbles were covered originating in the batch melting process. It is possible to trace the behavior of secondary bubbles, which occur where the glass contacts refractories and are entrapped in the feeder. In particular, the distribution of the gas concentration in the glass of the forming section is not so complex because there is no refining agent reaction. Accordingly, it might be possible to backtrack the bubble using data such as the location where the bubble exists, the bubble diameter and the gas composition.

f) Accurate glass properties at high temperatures are needed to lead to trustworthy conclusions from this simulation. Thermal conductivity, bulk expansion coefficient, viscosity and specific heat are necessary for thermal fluid calculation. Gas solubility, gas diffusivity and surface tension are also needed for the bubble removing evaluation. However, it is not an exaggeration to say that there are no reliable data nor ways of measuring these properties at present.

g) In this simulation, the target was to model the glass contact area in a glass furnace. However, many modeling themes in the glass contact field are still left for the researcher to deal with, for example: batch melting, bubbling, Joule heating by electricity, surface foaming and reboiling. In order to describe the overall process of glass melting, it is also necessary to make a model of radiant heat conduction by firing in the superstructure of a furnace.

*

The authors wish to express their sincere thanks to Mr. K. Kishida, Chairman of Nippon Electric Glass Co., Ltd., for his many years' encouragement of this work and permission to publish this paper. They extend their gratitude to Messrs. H. Nagao, M. Kato and Y. Sato (Nippon Electric Glass) for making the test models and carrying out experimental work, and also appreciate the cooperation of Messrs. H. Yoshikawa (Kouzou Keikaku Engineering, Tokyo) and S. Ikeuchi (Gauss Corporation, Osaka) in the field of computation.

3. References

[1] Kawachi, S.; Kawase, Y.: Evaluation of bubble removing performance in a TV glass furnace. Pt. 1. Mathematical formulation. Glastech. Ber. Glass Sci. Technol. **71** (1998) no. 4, p. 83–91.

[2] Amemiya, H.: Problems in glass melting process and the new development. In: Proc. 25th Summer Seminar for Young Ceramists, 1993, Ceram. Soc. Japan, Tokyo.

[3] Krämer, F.: Gasprofilmessungen zur Bestimmung der Gasabgabe beim Glasschmelzprozeß. Glastech. Ber. **53** (1980) no. 7, p. 177–188.

[4] Kawachi, S.; Kato, M.: Evaluation of reaction rate of refining agents. Glastech. Ber. Glass Sci. Technol. (In prep.)

[5] Mulfinger, H. O.: Gasanalytische Verfolgung des Läutervorganges im Tiegel und in der Schmelzwanne. Glastech. Ber. **49** (1976) no. 10, p. 232–245.

[6] Krämer, F.: Bubble defect diagnosis by means of a mathematical model. In: XIV International Congress on Glass, New Delhi (India) 1986. Coll. Papers. Vol. 2. p. 288–295.

0598P002

Addresses of the authors:

S. Kawachi
Nippon Electric Glass Co., Ltd.
Technology Department
7-1, Seiran, 2-Chome
Otsu, Shiga 520 (Japan)

Y. Kawase
Toyo University
Department of Applied Chemistry
Faculty of Engineering
Kujirai, Kawagoe-Shi, Saitama 350 (Japan)